CHEMICAL DETECTION FOR LAND MINING USING REMOTE SENSING BASED DEEP LEARNING

Murali Kalipindi[a]*, Ranichandra C[b], P.T.Kalaivaani[c], Senthilkumar N C[d], Veeramalai Sankaradass[e], Madiajagan M[f]

Article History: **Received:** 05.09.2022 **Revised:** 09.10.2022 **Accepted:** 10.11.2022

Abstract: The field of chemical hyperspectral (CHS) imaging is one that is still in the process of evolving, but it already has a wide range of applications in a variety of fields, including the military and the civilian sector. The detection and localization of materials based on the known spectrum properties of those materials is one application that may be carried out with the use of HS spectral data. In this paper, we develop a deep convolutional neural network to sense the minerals from the hyper spectral images using remote sensing. The images collected are used to classified using the deep learning model that classifies the instances and provides accurate results. The simulations are conducted to evaluate the efficacy of the model in detecting the minerals from the hyperspectral images. An accuracy of 92% is obtained during testing than other methods.

Keywords: Chemical Hyperspectral Imaging, Convolutional Neural Network, Remote Sensing

[a]. Associate Professor and HOD, Department of Artificial Intelligence and Machine Learning, Vijaya Institute of Technology for Women, Enikepadu, Andhra Pradesh, India.
[b]. Associate Professor, School of Information Technology and Engineering, Vellore Institute of Technology, Vellore, Tamil Nadu, India.
[c]. Associate Professor and Head, Department of ECE, Vivekanandha College of Engineering for Women (Autonomous), Tiruchengode, Namakkal, Tamil Nadu, India.
[d]. Associate Professor, School of Information Technology and Engineering, Vellore Institute of Technology, Vellore, Tamil Nadu, India.
[e]. Professor, Department of Computer Science and Engineering, Chennai Institute of Technology, Chennai, Tamil Nadu, India.
[f]. Associate Professor, School of Computer Science and Engineering, Vellore Institute of Technology, Vellore, Tamil Nadu, India

***Corresponding Author**

E-mail: kalipindimurali@gmail.com

DOI: 10.31838/ecb/2022.11.11.011

INTRODUCTION

The normally faint radiance that emanates from the chemical compounds of interest is effectively hidden and distorted as a result of the presence of a myriad of other light sources that are present in the clutter and environment. As a result, this endeavor is extremely difficult because it presents an extremely difficult challenge. Unmixing the data using the pure-pixel or endmember assumption that the target materials can be located in a few individual pixels without interference from other brightness sources is a common method for separating the radiance components that are present in the data. This assumption states that the target materials can be located in the few individual pixels. One other way that can be utilized is the examination of the likelihood ratio using a statistical methodology [1].

It is well knowledge that subpixel or mixed-pixel targets present a significant number of obstacles when contrasted with the more traditional endmember processing. The targets in question are either too small to be seen, or they are partially obscured by foliage or some other kind of cover. Both of these scenarios are possibilities. Statistical approaches such as adaptive matched detectors and adaptive subspace detectors are two examples of the kinds of approaches that can be utilized for this kind of objective. These two detectors both have adaptive capabilities. Both of these methods execute generalized likelihood ratio testing on the data by first whitening it with background sample covariance matrices and then projecting the data into the spectral subspace of the goal. This is done in order to determine whether or not the data meet the goal criteria. This is done in order to make certain that the statistics are accurate representations of the goal [2].

Remote sensing, geological field work, geophysical research, and geochemical surveys are some of the methods that are utilized in the process of mineral exploration. For a number of decades now, geologists have depended on remote sensing in order to locate mineralization by describing and delineating geological, structural, and lithological features. It is now possible, with the assistance of multispectral and/or hyperspectral sensors, as well as important advancements in the field of remotely sensed image analysis, to classify rocks and minerals into different categories according to the spectral characteristics they possess [3].

Mineral exploration has recently begun to make use of remote sensing, particularly in the form of the meticulous characterization of fault/fracture zones and/or minerals that have been subjected to hydrothermal alteration. This is done with the intention of achieving the aforementioned objective. These essential radicals are always present in minerals that are

formed by more sophisticated argillic alteration processes. The mineral products that come about as a result of propylitic alteration have a high absorption capability. These HAZs are grouped together in rings that spiral outward from the center of the ore and get progressively more intense as they move further away from the center [4]-[6].

Because of this, a GIS-based approach to the development of mineral potential maps using remote-sensing data has become a useful tool that is both efficient and accurate for the selection of target areas for mining exploration [7, 8]. Recent developments in GIS-based approaches to spatial analysis have resulted to improvements in pinpointing probable areas for the locations of hydrothermal mineral resource locations [9-10]. This is because mineral exploration relies heavily on GIS-based integration of spatially scattered remote-sensing data, which is a crucial component of the field of remote sensing. This is due to the fact that digital overlay techniques can be used to merge disparate information, which ultimately results in improved mineral prospecting maps [11].

Because each GIS predictive layer is given a weight that represents its significance in the process of modeling [12], the GIS-based knowledge-driven technique is excellent at producing predictive maps that are based on the decision of specialists. This is because the weights that are assigned to the GIS predictive layers are represented by their significance in the process. Additionally, in the prospective method of analysis, a relative value was assigned to each evidence map that displayed HAZs and/or fracture/fault zones. If we go with a plan that takes into account a number of different aspects, we can expect that the regions that have the highest aggregate weight after we have compiled the scores for all of the categories will be the ones in which we have the greatest likelihood of finding mineral and metal reserves.

RELATED WORKS

In order to map, Noori et al. [13] assessed a large number of image processing algorithms. Using ASTER data, they aimed to complete the mapping. Mineral assemblages formed as a result of hydrothermal alteration were found to be slightly different from those formed as a result of undisturbed rocks, and these differences were mapped. The research concluded that there are multiple analysis perform, and that a thorough exploration of the region should account for these.

The work of Guha et al. [14], who used emittance spectroscopy to examine the distribution of phosphate in carbonate-rich strata by data. Phosphorite was mapped and separated from its host-rock lithologies in this way. This image was instrumental in achieving the aims of this study. The RBD is also able to tell the difference between high- and low-quality phosphorite exposures. The authors suggest utilising the RBD of broadband ASTER thermal infrared (TIR) bands to research phosphorite in globally analogous geological systems.

Using ASTER data, Pour et al. [15] mapped out where listvenite occurs inside to extract spectral information for the goal of identifying alteration mineral assemblages and listvenites. It was done so that we could recognise listvenites and other minerals involved in the alteration process.

The goal was to figure out what drove gold mineralization here. However, the data fusion technique demonstrates that gold-quartz veins are more commonly seen in areas of chlorite-epidote alteration that coincide with dense lineament crossings. However, it does not appear that gold occurrences are spatially associated with any specific lithological units [16].

Sun et al. [17] combined geochemical data with ground-based hyperspectral imaging to mine sediment-hosted scattered gold. Combining this finding with information on geochemical processes required.

By combining information from a number of sensors on satellite images, Zoheir et al. [18] were able to create a picture, researchers were able to gain a more in-depth for performing more detail research which helps for understanding several investigation.

Pour et al. [19] used multispectral remote sensing data from Landsat-8, ASTER, and WorldView-3 to examine copper-gold mineralization at the regional, local, and district scales. This type of mineralization was discovered in Northwest Greenland Northeastern Inglefield Mobile Belt (IMB).

Bayesian networks were studied by Bolouki et al. [20] to determine if they might be used effectively in remote sensing of epithermal gold deposits, it was decided to employ a Bayesian network classifier.

Drill-core samples from the Bolcana porphyry copper-gold deposit were analysed for their mineral richness by Tușa et al. [21]. They did this by combining data from a mineral liberation analyzer with data from a scanning electron microscope and analysing the resulting images. When it was necessary to merge it using several machine learning algorithms were put into use. All of these techniques were put to good use. Somewhat quantitative data was plotted from drill-core samples.

The technique used band ratios and principal component analysis to create a map of the rearranged lithologies and minerals. It was decided to use this approach (PCA). Image processing methods were used to create the mineral prospectivity maps, and then fuzzy logic modelling was used to combine the many individual theme layers. At both the regional and district sizes, the most promising and economically promising zones of hydrothermal ore mineralization and carbonate-hosted Pb-Zn mineralization have been identified and highlighted. Carbonates were discovered to be the hosting material for these two forms of mineralization [22].

PROPOSED METHOD

The satellite photos were analyzed in order to get a better understanding of the specific location of the chromite resources. The preliminary exploration work that was carried out at the site began with the finding of harzburgite and dunite lithologies, which served as the first stage in the process. In the process of mapping ophiolites, two of the techniques that are recognized in the scientific community were utilized. These methodologies were the principal component analysis and a number of band rationing procedures. In the course of this investigation, the remote sensing research referred to a map of the local geology whenever it needed a point of reference. A step known as preprocessing had to be completed on the data set before it was possible to use those records in further processing. During this stage, the bands were adjusted in order to take into account a variety of factors, including the topography, the climate, the level of radioactivity, and the general form of the area.

When it came to the challenge of separating lithology units, using VNIR and SWIR data series proved to be extremely beneficial. Band ratio images, which were developed to demonstrate the spectral contrast of specific absorption

features, find widespread use in geological remote sensing as a result of the fact that their creation was predicated on the spectral reflectance of rocks and the minerals that compose them. Band ratio images were developed to demonstrate it. Band ratio analysis uses a wide range of different things in remote sensing, some examples of which are lithological mapping and mineral extraction. When doing exploration, band ratio can also be utilized as a method for locating serpentinite, dunite, and ophiolite harzburgite.

During the process of mapping ophiolite rocks, metabasalt, and metagabbro units, Amer utilized band ratios of (2 + 4)/3, (5 + 7)/6, and (7 + 9)/8. These band ratios were utilized in the process of differentiating ophiolite rocks from granite rocks. Because the authors came to the conclusion that the new band ratios are superior for recognizing and differentiating between ophiolitic lithological units as a result of their research, these ratios were used in this analysis. This conclusion was reached as a direct consequence of the author research. The mapping lithological features and the different types of alteration that may be found in metallogenic zones. This is done for the aim of extracting mineral deposits.

Principal component images were able to be computed utilizing this method as a result of establishing a correlation. This allowed for the computation of principal component images. As a consequence of this link, one is able, by means of analyzing the spectral information of the pixels, to identify whether or not those pixels that comprised the minerals of interest had high or low digital numbers (DNs). One of the discoveries that they made as a result of their investigation into the disparity between the lithology and the mineralized zones was this particular one.

Optimum Index Factor (OIF)

The optical intensity factor (OIF) for Bands 3, 6, and 8 was the greatest out of all of the VNIR and SWIR band combinations that were investigated for this study. The employment of a bigger number of bands led to an improvement in the spectral accuracy of the low-correlation bands, notably the thermal bands. This improvement was brought about by the expansion of the band count. It is necessary to calculate the OIF in order to produce high-quality false-color composites (colour combinations that have a higher OIF include more data):

$OIF=(\sum Si)/(\sum ri)$ (1)

where

Si - standard deviation, and

ri - bands correlation.

It is standard procedure to examine all of the colours in a spectrum in order to identify the deceptive colour combinations that conceal the most crucial information.

Spectral Angular Mapper (SAM) Algorithm

A core premise of the spectral angle mapping method is the concept that each pixel in an image acquired through remote sensing represents a distinct type of ground cover that can be placed into exactly one of these classes. This principle is central to the concept of spectral angle mapping. The algorithm operates under the assumption that this is one of the most essential variables. Examining the degree to which the two spectra are analogous to one another is one of the ways in which one can figure out how effective the SAM approach is.

The study has the option of using any number of the available spectra in order to build a spectral similarity. By calculating the angle that separates the spectra, we may be able to get an idea of how closely they are related to one another. Seeing the spectra as vectors in a space that has the same number of dimensions as the number of bands is the key to achieving this goal.

Using the HSI cube algorithm, each pixel vector in an HSI cube is assigned a name, and the names are selected by the spectral or spatial properties of the cube. The HSI can be formulated utilizing the mathematical notation that is as follows:

$X = [x1, x2,. . . , xB]T \in \mathbb{R}B\times(N\times M)$, (2)

where,

B - total bands.

$Y = fc(X,\theta)$ (3)

where,

fc(.) - mapping function

θ - adjustable parameter such that

$fc: X \rightarrow Y$ (4)

Deep Learning

In order to address the HSI classification problem, which needs the utilisation of CNN, 3D kernel is applied to images in order to extract spectral and spatial features from them. Utilizing 3D convolutional kernels is one way to accomplish the integrated feature mapping of input data with spectral and spatial dimensions. The formula for 3D convolution is presented in the following,

$$v_{ij}^{xy} = \Phi\left(b_{ij} + \sum_{m} \sum_{p=0}^{P_i-1} \sum_{q=0}^{Q_i-1} w_{ijm}^{pq} \times v_{(i-1)m}^{(x+p)(y+q)} \right) \quad (5)$$

where

(x, y, z) - current position

i - current operation,

j - jth feature map,

v_{ij}^{xy} - output position (x, y, z),

r - bias term,

k_{ijp}^{hwb} - connected weight value to jth feature map.

p - connected features,

f - activation function,

Bi, Hi and Wi – kernel size.

RESULTS AND DISCUSSIONS

We devised a technique that was predicated on deep metric learning in order to circumvent both the curse of dimensionality and the dearth of properly labelled training data. This allowed us to overcome both challenges simultaneously. Both of these issues were investigated using high-dimensional hyperspectral images in addition to several other sample sampling approaches. The results of these studies are presented below. To begin, in order to illustrate the effectiveness of the proposed algorithm, we carried out tests on three different open-source datasets. These experiments were carried out so that we could demonstrate the usefulness of the method. The following is an exhaustive overview of the images that were compiled following a search for them. Following that, an in-depth analysis of the model hyperparameters was carried out as in Figure 1-5.

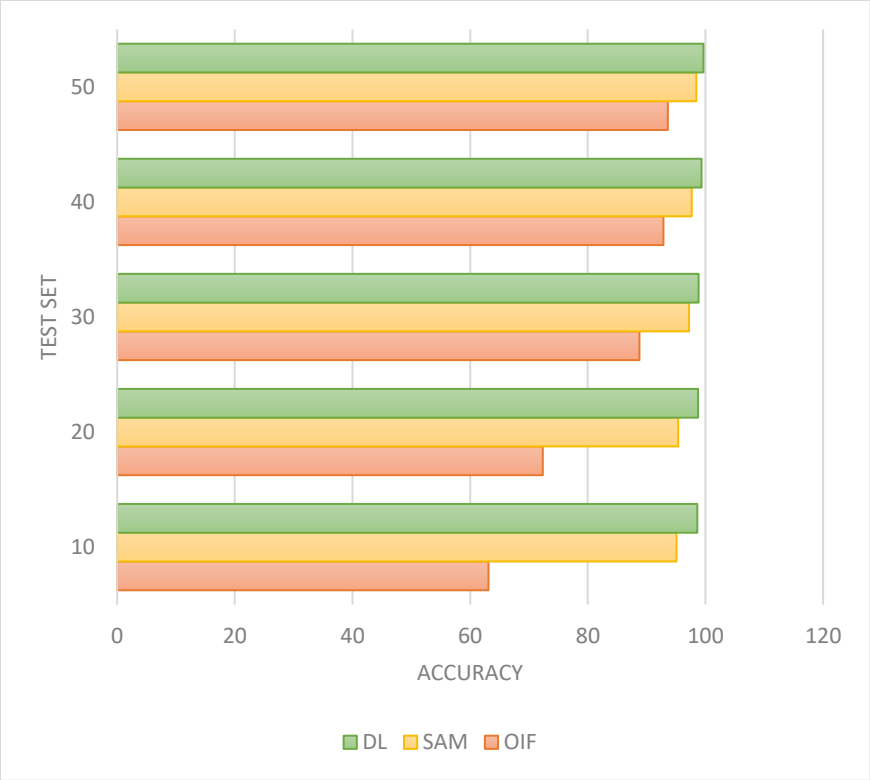

Figure 1: Accuracy of the CNN

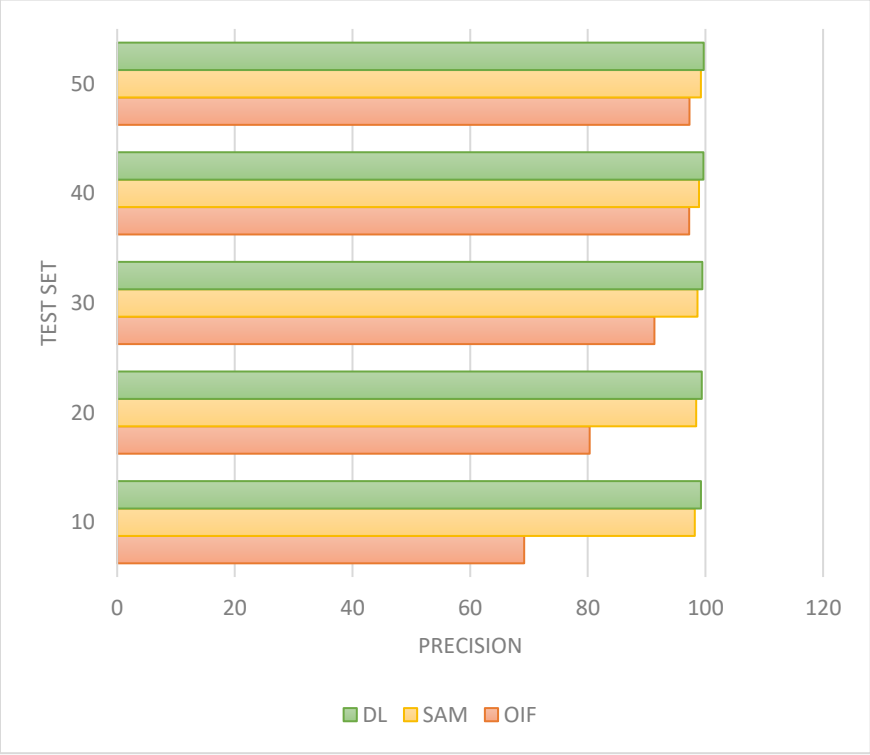

Figure 2: Precision of the CNN

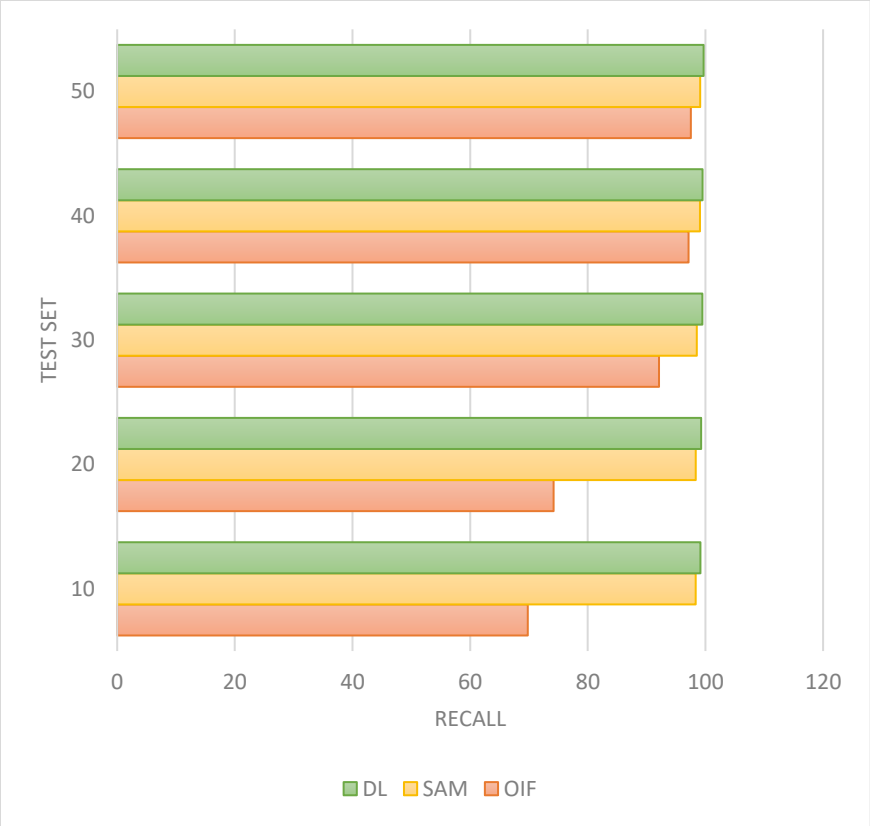

Figure 3: Recall of the CNN

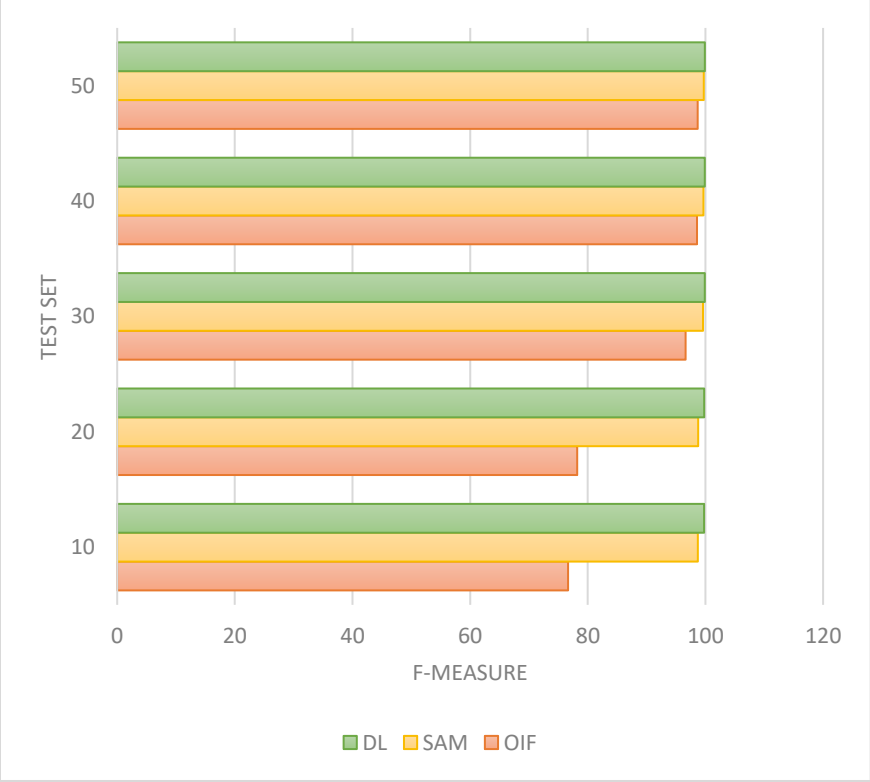

Figure 4: F-Measure of the CNN

Figure 5: MAPE

By utilizing an embedded network that was based on CNN, we were able to transform a high-dimensional feature space into a low-dimensional feature space that was simpler to work with. This made it possible for us to better handle the data. However, it was discovered that the usage of a CNN-based embedded network on its own was insufficient to accomplish the goals that were set. The utilization of an online triplet loss proved to be useful in either excessive or insufficient overfitting.

By applying enhanced sampling techniques to make the training of the network more targeted, we were able to achieve a greater dimensionality reduction effect with a lesser amount of data. This was made possible by the fact that we used fewer data.

This made it possible for us to achieve our goal of generating a higher effect with less data while still maintaining the advantages that CNN offers in its original form as a potent tool for dimensionality reduction. The effectiveness of CNN was assessed by employing three distinct categorization metrics on three distinct data sets. CNN displayed greater accuracy when compared to other possible categorization algorithms.

CONCLUSIONS

The deep networks were necessary in order to be successful in overcoming the obstacle of categorization when there were just a few tagged instances to work with. The improved performance of the network in classification tasks can be attributed to this ability of deep metrics, which has the capability to effectively make the same class more compact while simultaneously making the heterogeneous more distributed. In addition, the embedded network as a whole can be taught by utilizing the most challenging triplets that can be formed by the application of an online hard mining technique. This can be done by making use of the most difficult triplets. Because of this, the method that we showed performed better than competing algorithms on three different datasets when it came to the categorization of the data. In the process of classifying hyperspectral data using cross-entropy loss or other algorithms, other approaches differ from the way that we have presented in that they ignore the impact of intra-class distance in addition to the impact of inter-class distance. It is abundantly obvious that our strategy enhances the accuracy of classification as a result of the fact that it restricts the distance between classes as well as the distance within each class.

REFERENCES

i. Fan, Z., Zhan, T., Gao, Z., Li, R., Liu, Y., Zhang, L., ... & Xu, S. (2022). Land cover classification of resources survey remote sensing images based on segmentation model. IEEE Access.

ii. Bonicelli, L., Porrello, A., Vincenzi, S., Ippoliti, C., Iapaolo, F., Conte, A., & Calderara, S. (2022). Spotting Virus from Satellites: Modeling the Circulation of West Nile Virus Through Graph Neural Networks. arXiv preprint arXiv:2209.05251.

iii. Yuan, P., Zhao, Q., Zhao, X., Wang, X., Long, X., & Zheng, Y. (2022). A transformer-based Siamese network and an open optical dataset for semantic change detection of remote sensing

images. International Journal of Digital Earth, 15(1), 1506-1525.

iv. Paul, S., & Pal, S. (2022). Modelling hydrological strength and alteration in moribund deltaic India. Journal of Environmental Management, 319, 115679.

v. Saha, S., Shahzad, M., Ebel, P., & Zhu, X. X. (2022). Supervised Change Detection Using Pre-Change Optical-SAR and Post-Change SAR Data. IEEE Journal of Selected Topics in Applied Earth Observations and Remote Sensing.

vi. Lv, Z., Wang, F., Sun, W., You, Z., Falco, N., & Benediktsson, J. A. (2022). Landslide Inventory Mapping on VHR Images via Adaptive Region Shape Similarity. IEEE Transactions on Geoscience and Remote Sensing.

vii. Li, J., Liao, Y., Zhang, J., Zeng, D., & Qian, X. (2022). Semi-Supervised DEGAN for Optical High-Resolution Remote Sensing Image Scene Classification. Remote Sensing, 14(17), 4418.

viii. Chen, Z., Zhou, Y., Wang, B., Xu, X., He, N., Jin, S., & Jin, S. (2022). EGDE-Net: A building change detection method for high-resolution remote sensing imagery based on edge guidance and differential enhancement. ISPRS Journal of Photogrammetry and Remote Sensing, 191, 203-222.

ix. Matsui, K., & Kageyama, Y. (2022). Water pollution evaluation through fuzzy c-means clustering and neural networks using ALOS AVNIR-2 data and water depth of Lake Hosenko, Japan. Ecological Informatics, 70, 101761.

x. Wang, J. J., Dobigeon, N., Chabert, M., Wang, D. C., Huang, J., & Huang, T. Z. (2022). CD-GAN: a robust fusion-based generative adversarial network for unsupervised change detection between heterogeneous images. arXiv preprint arXiv:2203.00948.

xi. Li, H., Zhu, F., Zheng, X., Liu, M., & Chen, G. (2022). MSCDUNet: A Deep Learning Framework for Built-Up Area Change Detection Integrating Multispectral, SAR and VHR Data. IEEE Journal of Selected Topics in Applied Earth Observations and Remote Sensing.

xii. Abdullah, S. T., AL-Nuaimi, B. T., & Abed, H. N. (2022). A survey of deep learning-based object detection: Application and open issues. International Journal of Nonlinear Analysis and Applications, 13(2), 1495-1504.

xiii. Noori, L., Pour, A. B., Askari, G., Taghipour, N., Pradhan, B., Lee, C. W., & Honarmand, M. (2019). Comparison of different algorithms to map hydrothermal alteration zones using ASTER remote sensing data for polymetallic vein-type ore exploration: Toroud–Chahshirin Magmatic Belt (TCMB), North Iran. Remote Sensing, 11(5), 495.

xiv. Guha, A., Yamaguchi, Y., Chatterjee, S., Rani, K., & Vinod Kumar, K. (2019). Emittance spectroscopy and broadband thermal remote sensing applied to phosphorite and its utility in geoexploration: A study in the parts of Rajasthan, India. Remote Sensing, 11(9), 1003.

xv. Pour, A. B., Park, Y., Crispini, L., Läufer, A., Hong, J. K., Park, T. Y. S., ... & Rahmani, O. (2019). Mapping Listvenite Occurrences in the Damage Zones of Northern Victoria Land, Antarctica Using ASTER Satellite Remote Sensing Data. Remote Sens. 11, 1408.

xvi. Zoheir, B., Emam, A., Abdel-Wahed, M., & Soliman, N. (2019). Multispectral and radar data for the setting of gold mineralization in the South Eastern Desert, Egypt. Remote Sensing, 11(12), 1450.

xvii. Sun, L., Khan, S., & Shabestari, P. (2019). Integrated hyperspectral and geochemical study of sediment-hosted disseminated gold at the Goldstrike District, Utah. Remote sensing, 11(17), 1987.

xviii. Zoheir, B., El-Wahed, M. A., Pour, A. B., & Abdelnasser, A. (2019). Orogenic gold in transpression and transtension zones: Field and remote sensing studies of the barramiya–mueilha sector, Egypt. Remote Sensing, 11(18), 2122.

xix. Pour, A. B., Park, T. Y., Park, Y., Hong, J. K., Muslim, A. M., Laufer, A., ... & Hossain, M. S. (2019). Landsat-8, Advanced Spaceborne Thermal Emission and Reflection Radiometer, and WorldView-3 Multispectral Satellite Imagery for Prospecting Copper-Gold Mineralization in the Northeastern Inglefield Mobile Belt (IMB). Northwest Greenland. Remote Sens. 11, 2430.

xx. Bolouki, S. M., Ramazi, H. R., Maghsoudi, A., Beiranvand Pour, A., & Sohrabi, G. (2019). A remote sensing-based application of Bayesian networks for epithermal gold potential mapping in Ahar-Arasbaran Area, NW Iran. Remote Sensing, 12(1), 105.

xxi. Tuşa, L., Khodadadzadeh, M., Contreras, C., Rafiezadeh Shahi, K., Fuchs, M., Gloaguen, R., & Gutzmer, J. (2020). Drill-core mineral abundance estimation using hyperspectral and high-resolution mineralogical data. Remote Sensing, 12(7), 1218.

xxii. Sekandari, M., Masoumi, I., Beiranvand Pour, A., M Muslim, A., Rahmani, O., Hashim, M., ... & Aminpour, S. M. (2020). Application of Landsat-8, Sentinel-2, ASTER and WorldView-3 spectral imagery for exploration of carbonate-hosted Pb-Zn deposits in the Central Iranian Terrane (CIT). Remote Sensing, 12(8), 1239.